OPEN EUROPEAN JOURNAL ON VARIABLE STARS
http://oejv.physics.muni.cz
June 2021 DOI: 10.5817/OEJV2021-0217 ISSN 1801–5964

GSC 03588-09315 IS A LOW-AMPLITUDE DELTA SCUTI VARIABLE

Christopher Lloyd[1], Yenal Öğmen[2,7], Gary Walker[3,7], Kenneth Menzies[4,7], Geoffrey Stone[5,7], David Boyd[6,8]

1) Department of Physics and Astronomy, University of Sussex, Brighton, BN1 9QH C.Lloyd@sussex.ac.uk
2) CBA Cyprus, Green Island Observatory, Gecitkale, North Cyprus yenalogmen@yahoo.com
3) Maria Mitchell Observatory, Nantucket, MA 02554
4) 318A Potter Road, Framingham, MA 01701
5) 9 Wildflower Way, Santa Fe, NM 87506
6) West Challow Observatory, Silver Lane, West Challow, OX12 9TX
7) American Association of Variable Star Observers, 49 Bay State Rd. Cambridge, MA 02138
8) BAA Variable Star Section, Burlington House, Piccadilly, London, W1J 0DU

Abstract: Time-series observations of GSC 03588-09315 show it is a very low amplitude, multiperiodic delta Scuti variable at the limit of detectability. Five frequencies have been identified at 13.86819(24), 8.10026(79), 5.01966(79), 11.67281(55) and 8.17490(59) cycles d^{-1} with amplitudes of 10, 5, 5, 4, and 3 mmag respectively. The spectral energy distribution of the star is very closely matched to a spectral type of F0V, but it is probably $1\overset{\mathrm{m}}{.}3$ brighter than a main-sequence star, so is likely to be evolved.

1 Introduction

GSC 03588-09315 (2MASS J21031315+4627588, UCAC4 683-095248, 21 03 13.16 +46 27 58.8 J2000) was found to be a low-amplitude variable by Öğmen (see Öğmen & Lloyd, 2019) while making observations of the recently discovered WZ Sge-type dwarf nova TCP J21040470+4631129. The star had a full amplitude of $0\overset{\mathrm{m}}{.}02$ in V and the principal frequency was quickly identified as, $f_1 = 13.86819(24)$ cycles d^{-1}. It was also clear that the star was multiperiodic so in a bid to reduce the aliasing problems additional observations were make from several sites.

2 Observations

Photometric observations were made from one site in Cyprus and three in the USA, and ran from 2019 July 12 to 2020 April 23 with a seasonal gap from October to December. Most of the images were taken with a V filter but some runs were unfiltered. All the images were bias-, dark-subtracted and flat fielded, and the reduced using aperture photometry software packages API4Win or MAXIM DL. The magnitudes were obtained by calibration relative to a local sequence of comparison stars to give V, or in the case of the unfiltered images, reduced as V, to give CV magnitudes. In total over 74 hours of observations were made on 24 nights in runs up to seven hours in length. The runs longer than one hour are listed in Table 1 and all the data are available from the AAVSO archive.

Table 1: Observing log of the longer time-series runs

Date	JD	Hours	Observer	Band	N
2019 Jul 12	2458677.346 - .478	3.2	Öğmen	V	353
2019 Jul 15	2458680.251 - .426	4.2	Öğmen	V	399
2019 Jul 17	2458682.272 - .439	4.0	Öğmen	V	200
2019 Jul 19	2458684.251 - .418	4.0	Öğmen	V	197
2019 Jul 22	2458687.250 - .417	4.0	Öğmen	V	200
2019 Jul 25	2458690.250 - .420	4.1	Öğmen	V	200
2019 Jul 28	2458693.250 - .418	4.0	Öğmen	V	200
2019 Aug 02	2458697.739 - .869	3.1	Menzies	V	145
2019 Aug 05	2458700.562 - .870	7.4	Menzies	V	320
2019 Aug 14	2458710.235 - .401	4.0	Öğmen	V	200
2019 Aug 18	2458714.242 - .412	4.1	Öğmen	V	199
2019 Aug 20	2458716.232 - .403	4.1	Öğmen	V	198
2019 Aug 29	2458725.226 - .400	4.2	Öğmen	V	200
2019 Sep 22	2458748.725 - .858	3.2	Walker	V	90
2019 Sep 26	2458752.731 - .863	3.2	Walker	V	90
2019 Oct 01	2458757.651 - .904	6.1	Walker	V	158
2019 Dec 15	2458832.537 - .586	1.2	Stone	CV	100
2019 Dec 16	2458833.536 - .585	1.2	Stone	CV	100
2019 Dec 17	2458834.537 - .589	1.2	Stone	CV	100
2019 Dec 26	2458843.540 - .588	1.2	Stone	CV	93

In addition to the photometry a low resolution (5Å) spectrum covering the wavelength range $\lambda\lambda 4000 - 7000$ Åwas taken on 2019 August 19 UT (JD 2458715) using a Shelyak Instruments LISA spectrograph. The spectrum was bias-, dark-subtracted and flat fielded, and wavelength calibrated using the spectrograph's internal Ar-Ne lamp. It was flux corrected for the instrumental and atmospheric response using spectra of an A-type star with a measured spectrum observed at a similar air mass, and absolutely calibrated using the known V magnitude. For details of this process see Boyd (2020), The details of all the instruments used are given in Table 2.

Additional data are taken from the All-Sky Automated Survey for Supernovae (ASAS-SN) archives (Shappee et al., 2014; Kochanek et al., 2017), which provides up to three V or g-band magnitudes every few days throughout the observing season. Multiple observations are typically made in the space of $0^{\rm d}.003$ or 4 minutes, although for various operational

Table 2: List of equipment used

Observer	Telescope	Camera	Filter
Boyd	0.28-m SCT	LISA spectrograph + SXVR-H694	
Menzies	0.317-m modified Harmer-Wynne Cass.	SBIG STL-6303E	V
Öğmen	Meade 0.35-m LX200R SCT	SBIG ST8XME	V
Stone	0.43-m f/6.8 Corrected Dall-Kirkham	SBIG STXL-11002	V/CV
Walker	0.51-m Planewave CDK	FLI Kepler KL400 sCMOS	V

OPEN EUROPEAN JOURNAL ON VARIABLE STARS
http://oejv.physics.muni.cz
June 2021 DOI: 10.5817/OEJV2021-0217 ISSN 1801–5964

reasons not all of these survive, so on average $\sim 75\%$ of the groups contain three points. Occasionally several groups are made in one night. The points in each group were averaged to produce mean values. Observations are available from 2015 to 2018 in the V-band and from 2018 to the present with the SDSS g filter.

3 Results

The data have been analysed by repeated application of a period search – fitting and subtraction loop until the noise level has been reached. Frequencies were identified through both a Discrete Fourier Transform (DFT) and a Lomb-Scargle periodogram, and then refined and removed using a multi-frequency Fourier fitting routine of the form

$$V_k = \sum_{j=1}^{m} a_j \cos(2\pi f_j T_k + \phi_j) + c_z \tag{1}$$

where V_k is the observed magnitude at time T_k, $j = 1, ..., m$ is the number of frequencies, and there is just the single harmonic for each frequency, ϕ_j is the phase offset for each

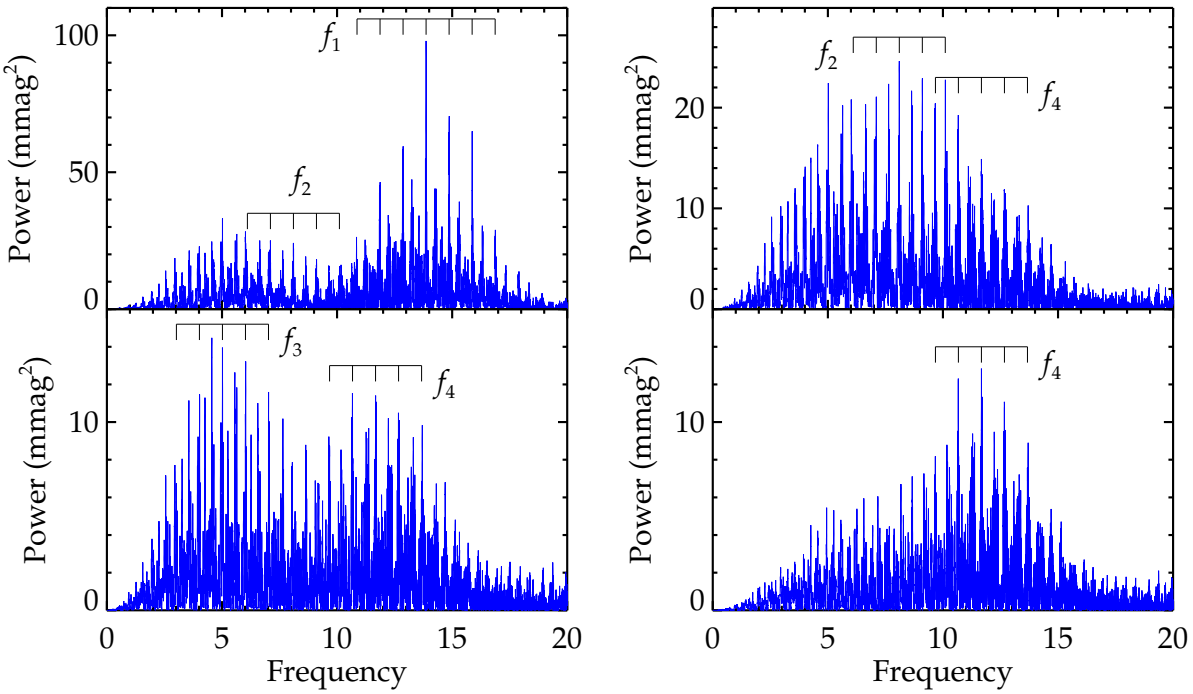

Figure 1: Discrete Fourier Transform (DFT) periodogram of the time-series data prior to the removal of each frequency. The principal frequency, $f_1 = 13.86819(24)$ is clearly visible in the top-left panel and is identified with its aliases at ± 1, 2 and 3 cycles d^{-1}. The likely second frequency, $f_2 = 8.10026(79)$ and its aliases are also identified but appear more clearly in the top-right panel. The confusion around f_2 is probably caused by the overlapping structures associated with two weaker frequencies, f_3 and f_4 near 5 and 12 cycles d^{-1}. The bottom-left panel shows the preferred $f_3 = 5.01966(79)$ (see text for details) and aliases, together with the structure associated with $f_4 = 11.67281(55)$, which appears more clearly in the bottom-right panel.

frequency j, and c_z is the constant level for any particular subset of the data.

The time-series data were analysed using offsets for the individual runs and also grouped by observer. Although f_1 was clearly identified using the observer offsets there was significant power at the lowest frequencies indicating that night-to-night variation was still important even for V-band data. Using the data offsets obviously eliminated the low-frequency features but some runs had to be filtered to equalize the noise levels between runs. Various schemes of selecting and filtering the data were examined and for all these f_1 was clear and unambiguous with $f_1 = 13.86819(24)$ cycles d^{-1} and a (sinusoidal, a_1) amplitude of $0\overset{\mathrm{m}}{.}010$.

The DFT periodograms of the time-series data are shown in Figure 1 as these give a direct indication of the power, as opposed to the relative scale of the Lomb-Scargle periodograms. Both methods produce almost identical results apart from one mentioned below. The principal frequency is clearly visible with its 1-day aliases as the four next most significant features. The noise level at 20 cycles d^{-1} continues to higher frequencies so there are no significant overtones of f_1 in the data. When f_1 is removed there is a broad confusion of significant features from $\sim 5 - 10$ cycles d^{-1}.

The strongest and most persistent frequency is $f_2 = 8.10026(79)$ with an amplitude of $0\overset{\mathrm{m}}{.}005$, which appears with its close 1-day aliases. However, the discrimination between these is not high. After the removal of f_2 there are two clusters of frequencies near 5 and 12 cycles d^{-1}, both with amplitudes only marginally weaker than f_2. The lower frequency could be a manifestation of diurnal or extinction related variations, or it could be a real frequency in the γ Doradus range. Either way it cannot be identified unambiguously as the features here belong to two series' of aliases with similar power. The preferred value is $f_3 = 5.01966(79)$ as this feature dominates this region in the two earlier periodograms, and it appears with a number of its 1-day aliases. It is also the dominant frequency in the Lomb-Scargle periodogram at this level. Ultimately this combination of frequencies also leads to the minimum χ^2 solution and the lowest residual power in the periodogram. Ironically, the fourth frequency $f_4 = 11.67281(55)$ and its 1-day aliases appear more stable

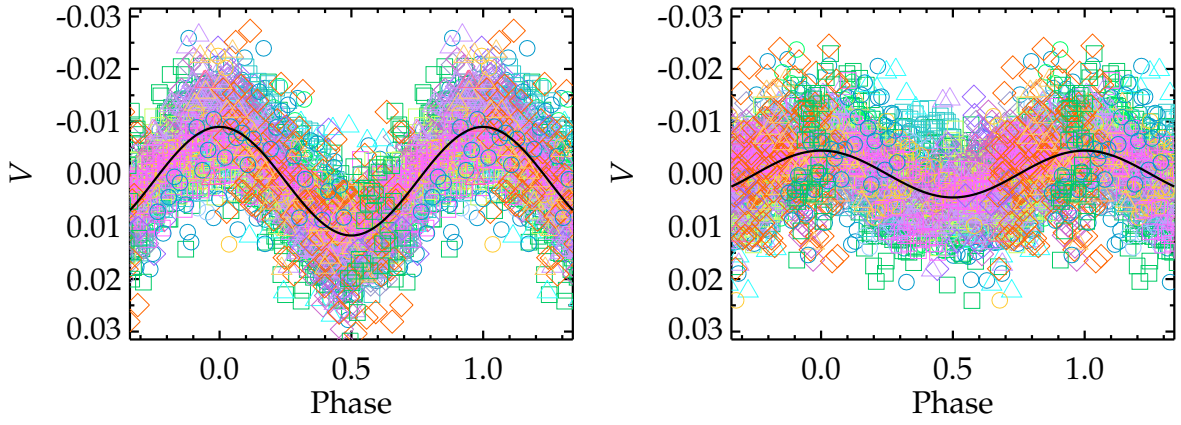

Figure 2: Phase diagram of the time-series data folded on the principal frequency, $f_1 = 13.86819(24)$ cycles d^{-1} (left), and the likely second frequency, $f_2 = 8.10026(79)$ cycles d^{-1} (right).

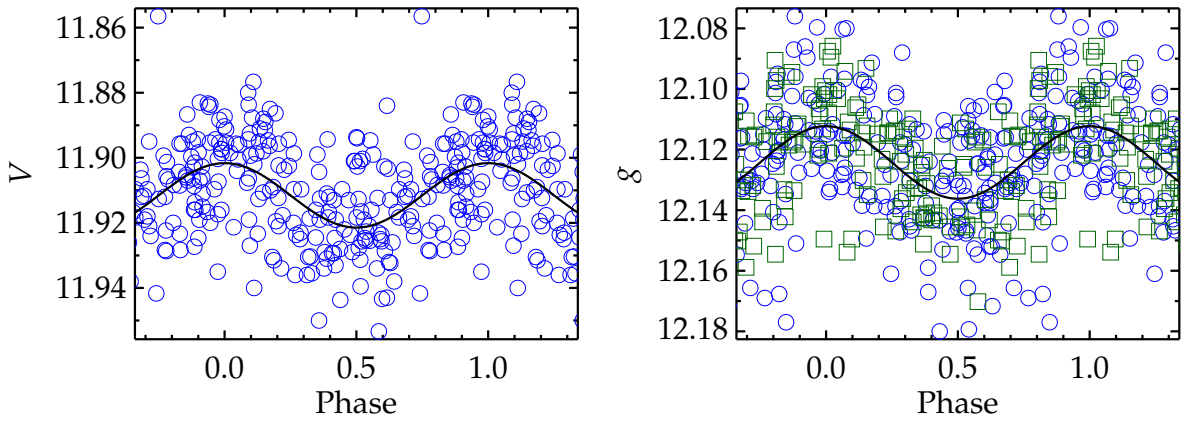

Figure 3: Phase diagram of the ASAS-SN V-band (left) data folded on $f = 13.86809$ and (right) ASAS-SN g-band data folded on $f = 13.86839$ cycles d^{-1}. The different cameras are shown in different colours.

and are insensitive to the exact value of f_3 that is removed. A fifth frequency has been identified at $f_5 = 8.17490(59)$ but this is more in the realm of speculation, and although it is not the strongest feature of the periodogram it does appear with a number of its 1-day aliases. It is the most likely feature at this level but is included mostly to illustrate the scale of activity close to the noise limit. So, it is possible to say with some confidence that f_1 is clearly identified, f_2 is probably correct, f_3 maybe correct, but it could be some other feature ~ 5 cycles d^{-1}, and f_4 is very likely. At the noise limit f_5 seems the most likely but this is little more than speculation. After the removal of five frequencies the remaining power is equivalent to an amplitude of $< 0\overset{\mathrm{m}}{.}0022$ and the residuals of the 5-frequency fit have $\sigma = 0\overset{\mathrm{m}}{.}0062$. The periodogram of these residuals again shows two frequency ranges around 3–7 and 9–15 cycles d^{-1} suggesting further, possibly real, very weak features contributing to the noise. The time-series data folded on f_1 and f_2 are shown in Figure 2. The frequencies do not show the standard radial-pulsator ratios so the star is most likely a non-radial pulsator.

The ASAS-SN data were treated the same way although cameras offsets were only applied to the g-band data as they were taken with two cameras, and the V data with just one. Remarkably, the principal frequency can be identified in both bands at $f = 13.86809(11)$ in V and $f = 13.86839(11)$ cycles d^{-1} in g, with amplitudes of $0\overset{\mathrm{m}}{.}010$ and $0\overset{\mathrm{m}}{.}012$ respectively. There is no sign of f_2 in the ASAS-SN data, however, there is a

Table 3: Frequency Table of the time-series data

f	Frequency(σ)	Amplitude $a_j(\sigma)$
f_1	13.86819(24)	0.0103(3)
f_2	8.10026(79)	0.0045(3)
f_3	5.01966(79)	0.0052(3)
f_4	11.67281(55)	0.0039(3)
f_5	8.17490(59)	0.0032(3)

June 2021 DOI: 10.5817/OEJV2021-0217 ISSN 1801–5964

weak feature common to both the V and g data at $f = 11.692$ which is close to f_4. The ASAS-SN data folded on f_1 are shown in Figure 3.

4 Spectral Energy Distribution and Luminosity

The low-resolution spectrum of the variable is absolutely calibrated in terms so it retains information on the spectral energy distribution (SED) of the star. It has been compared with standard spectra from Pickles (1998) Stellar Flux Library using a minimization scheme that also fits the reddening. The best fit is found for the F0 V library spectrum with $E_{\mathrm{B-V}} = 0.20$, and is shown in Figure 4. The G8 V spectrum is a very poor fit and both the F2 V and F0-2 IV spectra give about twice the χ^2 of the best fit. Later spectral types also require zero or negative reddening for an adequate fit so are even less likely.

The SED has also been determined from the available photometric data and again these have been compared with the Stellar Flux Library spectra. Magnitudes have been taken from *Tycho* $B_{\mathrm{T}}V_{\mathrm{T}}$ (Høg et al., 2000), Carlsberg Meridian Catalogue 15 r', (Niels Bohr Institute et al., 2014), APASS DR9 BV and $g'r'i'$ (Henden et al., 2015) TASS Johnson-Cousins VI_{C} (Droege et al., 2006), *Gaia* EDR3 G, BP, RP (Gaia Collaboration, 2020), Pan-STARRS *grizy* (Chambers et al., 2016), 2MASS JHK_{s} (Cutri et al., 2003; Skrutskie et al., 2006) and WISE $W1$, $W2$, $W3$, and $W4$ (Wright et al., 2010; Cutri & et al., 2014). In the same way as with the spectrum above the best fit between the library spectra and the observed fluxes has been determined by a minimization scheme which also fits the reddening. The best fit was again found with a spectral type of F0 V, which was marginally better than adjacent spectra, and $E_{\mathrm{B-V}} = 0.19$, also similar to the earlier value. The only other photometrically derived spectral type is F8 IV from

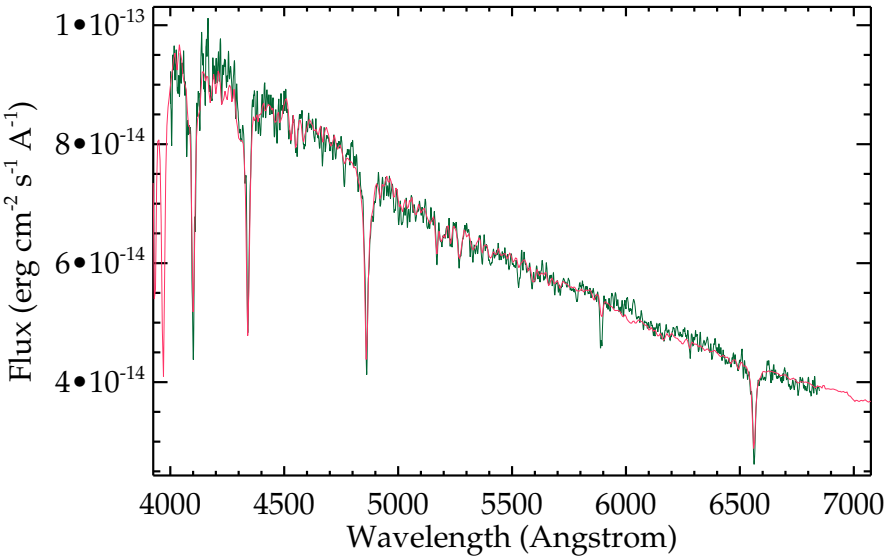

Figure 4: The observed absolutely calibrated, low-resolution spectrum of GSC 03588-09315 dereddened with $E_{\mathrm{B-V}} = 0.2$ (green) overlayed with the‘ F0 V library spectrum from Pickles (red).

OPEN EUROPEAN JOURNAL ON VARIABLE STARS
http://oejv.physics.muni.cz
June 2021 DOI: 10.5817/OEJV2021-0217 ISSN 1801–5964

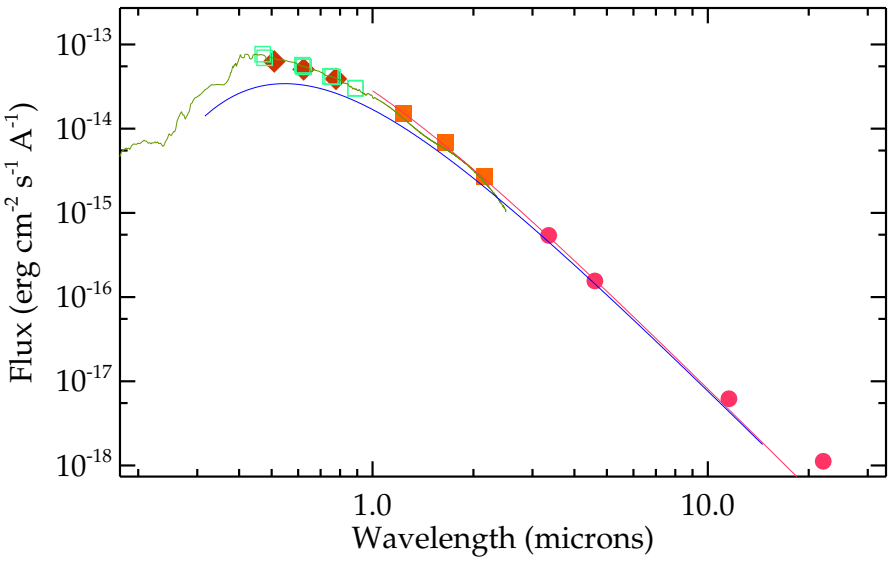

Figure 5: Spectral energy distribution from the photometric sources given in the text. The green line is the best fit F0 V spectrum and the red line is the black-body curve of 7220 K longward of 1 micron. The blue line shows the 5300 K black-body curve from 0.3 microns

Pickles & Depagne (2010). While this is a reasonable fit to the data it does require zero reddening. There are rather more photometric estimates of the temperature of the star but these show a wide range from $T_{\rm eff}$ = 5322 K (Ammons et al., 2006), $T_{\rm eff}$ = 5997 K (*Gaia* DR2 Gaia Collaboration et al., 2018), $T_{\rm eff}$ = 6091 K (*Gaia* DR1 McDonald et al., 2017), $T_{\rm eff}$ = 6803 K (*StarHorse* Anders et al., 2019), to $T_{\rm eff} = 7224 \pm 371$ K (*Gaia* DR2 Bai et al., 2019), although most are based on *Gaia* data. These cover the spectral type range from K0 – F0. The spectral energy distribution is shown in Figure 5 with the F0 V spectrum and black-body curves for 5500 K and 7220K. There appears to be a slight infra-red excess beyond 10 microns.

The position of GSC 03588-09315 places it at $l = 87.6$, $b = -0.2$, very close to the galactic plane so extinction will be high. The NASA/IPAC Infrared Science Archive gives the total reddening in this direction as $E_{\rm B-V} = 1.6 - 1.8$ (Schlegel et al., 1998; Schlafly & Finkbeiner, 2011) suggesting $A_{\rm V} \sim 5$ magnitudes. However, *Gaia* provides a distance of 1032 ± 12 pc (Gaia Collaboration, 2020; Bailer-Jones et al., 2021) and the 3D Dust Maps of Green et al. (2019) and Lallement et al. (2018) suggest that the bulk of the reddening occurs beyond 2 kpc. Using Green et al.'s Bayestar19 calibration, $E_{\rm B-V} = 0.94 \pm 0.06 E_{\rm g-r}$, with $E_{\rm g-r} = 0.20 \pm 0.02$ at 1032 pc, $E_{\rm B-V} = 0.19 \pm 0.03$, . Lallement et al. find a slightly higher reddening, $E_{\rm B-V} = 0.26 \pm 0.09$, so taking $E_{\rm B-V} = 0.20 \pm 0.03$ and $R_{\rm V} = 3.1$ this gives $A_{\rm V} = 0.6 \pm 0.1$. When combined with the distance and magnitude, taken as $V = 11.91$, this yields an absolute magnitude of $M_{\rm V} = 1.24 \pm 0.10$. According to the Rochester calibration this absolute magnitude corresponds to an A0-1 main sequence star (see Pecaut & Mamajek, 2013, for details). If the star is F0 as the fitting suggests then it is about $1\overset{\rm m}{.}3$ brighter than a main-sequence star, so is most likely evolved.

June 2021 DOI: 10.5817/OEJV2021-0217 ISSN 1801–5964

5 Conclusion

Time-series observations of GSC 03588-09315 show it is a very low amplitude, multiperiodic δ Scuti variable at the limit of detectability for modest, ground-based telescopes. Five frequencies have been identified at 13.86819(24), 8.10026(79), 5.01966(79), 11.67281(55) and 8.17490(59) cycles d^{-1} with amplitudes of 10, 5, 5, 4, and 3 mmag respectively. The last is at the noise limit but it seems likely that other frequencies are present. The ASAS-SN V and g-band data also show the principal frequency. A flux-calibrated spectrum and the photometrically derived spectral energy distribution both suggest that the star has a spectral type of F0V with $E_{\mathrm{B-V}} = 0.2$. The same reddening is also suggested by the 3D Dust Maps out to the *Gaia* distance of 1032 pc. The distance, magnitude and reddening combine to suggest $M_{\mathrm{V}} = 1.24$, which is about $1\overset{\mathrm{m}}{.}3$ brighter than an F0 main-sequence star and further supports the view that this is a δ Scuti variable.

Acknowledgements: This publication makes use of data products from the Two Micron All Sky Survey, which is a joint project of the University of Massachusetts and the Infrared Processing and Analysis Center/California Institute of Technology, funded by the National Aeronautics and Space Administration and the National Science Foundation. This publication makes use of data products from the Wide-field Infrared Survey Explorer, which is a joint project of the University of California, Los Angeles, and the Jet Propulsion Laboratory/California Institute of Technology, funded by the National Aeronautics and Space Administration. The authors are pleased to acknowledge use of NASA's Astrophysics Data System Bibliographic Services. This research has made use of the SIMBAD database and the VizieR catalogue access tool, CDS, Strasbourg, France (DOI: 10.26093/cds/vizier).

References

Ammons, S. M., Robinson, S. E., Strader, J., et al., 2006, *ApJ*, **638**, 1004
Anders, F., Khalatyan, A., Chiappini, C., et al., 2019, *A&A*, **628**, A94
Bai, Y., Liu, J., Bai, Z., et al., 2019, *AJ*, **158**, 93
Bailer-Jones, C. A. L., Rybizki, J., Fouesneau, M., et al., 2021, *AJ*, **161**, 147
Boyd, D., 2020, A method of calibrating spectra in absolute flux using V magnitudes
Chambers, K. C., Magnier, E. A., Metcalfe, N., et al., 2016, *arXiv e-prints*, arXiv:1612.05560
Cutri, R. M. & et al., 2014, *VizieR Online Data Catalog*, II/328
Cutri, R. M., Skrutskie, M. F., van Dyk, S., et al., 2003, *VizieR Online Data Catalog*, II/246
Droege, T. F., Richmond, M. W., Sallman, M. P., et al., 2006, *PASP*, **118**, 1666
Gaia Collaboration, 2020, *VizieR Online Data Catalog*, I/350
Gaia Collaboration, Brown, A. G. A., Vallenari, A., et al., 2018, *A&A*, **616**, A1
Green, G. M., Schlafly, E., Zucker, C., et al., 2019, *ApJ*, **887**, 93
Henden, A. A., Levine, S., Terrell, D., et al., 2015, in *American Astronomical Society Meeting Abstracts*, vol. 225, p. 336.16

Høg, E., Fabricius, C., Makarov, V. V., et al., 2000, *A&A*, **355**, L27
Kochanek, C. S., Shappee, B. J., Stanek, K. Z., et al., 2017, *PASP*, **129**, 104502
Lallement, R., Capitanio, L., Ruiz-Dern, L., et al., 2018, *A&A*, **616**, A132
McDonald, I., Zijlstra, A. A., & Watson, R. A., 2017, *MNRAS*, **471**, 770
Niels Bohr Institute, Institute of Astronomy, Cambridge, & Real Instituto y Observatorio de La Armada, 2014, *VizieR Online Data Catalog*, I/327
Öğmen, Y. & Lloyd, C., 2019, Variability of GSC 03588-09315
Pecaut, M. J. & Mamajek, E. E., 2013, *ApJ Suppl*, **208**, 9
Pickles, A. & Depagne, É., 2010, *PASP*, **122**, 1437
Pickles, A. J., 1998, *PASP*, **110**, 863
Schlafly, E. F. & Finkbeiner, D. P., 2011, *ApJ*, **737**, 103
Schlegel, D. J., Finkbeiner, D. P., & Davis, M., 1998, *ApJ*, **500**, 525
Shappee, B. J., Prieto, J. L., Grupe, D., et al., 2014, *ApJ*, **788**, 48
Skrutskie, M. F., Cutri, R. M., Stiening, R., et al., 2006, *AJ*, **131**, 1163
Wright, E. L., Eisenhardt, P. R. M., Mainzer, A. K., et al., 2010, *AJ*, **140**, 1868